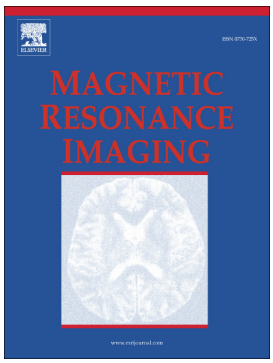

Microstructural features assessment of different waterlogged wood species by NMR diffusion validated with complementary techniques

V. Stagno, F. Egizi, F. Corticelli, V. Morandi, F. Valle, G. Costantini, S. Longo, S. Capuani

PII: S0730-725X(21)00140-5

DOI: https://doi.org/10.1016/j.mri.2021.08.010

Reference: MRI 9660

To appear in: *Magnetic Resonance Imaging*

Received date: 21 March 2021

Revised date: 27 July 2021

Accepted date: 25 August 2021

Please cite this article as: V. Stagno, F. Egizi, F. Corticelli, et al., Microstructural features assessment of different waterlogged wood species by NMR diffusion validated with complementary techniques, *Magnetic Resonance Imaging* (2018), https://doi.org/10.1016/j.mri.2021.08.010

Microstructural features assessment of different waterlogged wood species by NMR Diffusion validated with complementary techniques

V. Stagno[1,2], F. Egizi[2] , F. Corticelli[3], V. Morandi[3], F. Valle[4], G. Costantini[2], S. Longo[2,5], S. Capuani[2,6,*] *silvia.capuani@isc.cnr.it*

[1]Department of Earth Sciences, Sapienza University of Rome, Piazzale Aldo Moro 5, 00185 Rome, Italy.

[2]National Research Council - Institute for Complex Systems (CNR-ISC) c/o Physics Department Sapienza University of Rome, Rome, Italy.

[3]Consiglio Nazionale delle Ricerche - Istituto per la Microelettronica e Microsistemi (CNR-IMM) Bologna, P. Gobetti 101, 40129 Bologna, Italy.

[4]Consiglio Nazionale delle Ricerche - Istituto per lo Studio dei Materiali Nanostrutturati (CNR-ISMN) Bologna, P. Gobetti 101, 40129 Bologna, Italy.

[5]Department of Mathematical and Computational Sciences, Physics Science and Earth Sciences (MIFT), University of Messina, Messina 98166, Italy.

[6]Centro Fermi - Museo Storico della Fisica e Centro Studi e Ricerche Enrico Fermi Piazza del Viminale 1, 00184 Rome, Italy.

[*]Corresponding author.

Abstract

Wood is a hygroscopic, multi-scale and anisotropic natural material composed of pores with different size and differently oriented. In particular, archaeologically excavated wood generally is waterlogged wood with very high moisture content (400%–800%) that need to have a rapid investigation at the microstructural level to obtain the best treatment with preservative agents. Time-dependent diffusion coefficient D(t) quantified by Pulse Field Gradient (PFG) Nuclear Magnetic Resonance (NMR) techniques provides useful information about complex porous media, such as the tortuosity (τ) describing pore connectivity and fluid transport through media. the average-pore size, the anisotropic degree (a_n). However, diffusion NMR is intrinsically limited since it is an indirect measure of medium microstructure and relies on inferences from models and estimation of relevant diffusion parameters. Therefore, it is necessary to validate the information obtained from NMR diffusion parameters through complementary investigations. In this work, the structures of five waterlogged wood species were studied by PFG of absorbed water. D(t) and τ of water diffusing along and perpendicular to vessels/tracheids main axes together with relaxation times and a_n were quantified. From these parameters, the pore sizes distribution and the wood microstructure characterization were obtained. Results among wood species were compared, validated and integrated by micro-imaging NMR (μ-MRI), environmental-scanning electron-microscope (ESEM) images, wood dry density and imbibition times measurement of all woods. The work suggests that a_n *vs* τ rather than the estimated pore size diversifies and characterize the different wood species. As a consequence diffusion-anisotropy *vs* tortuosity could be an alternative method to characterize and differentiate wood species of waterlogged wood when high resolution images (μ-MRI and ESEM)

are not available. Moreover, the combined use of D(t) and micro-MRI expands the scale of dimensions observable by NMR covering all the interesting length scales of wood.

Keywords

- Softwood and Hardwood
- Wood Tortuosity
- Diffusion NMR
- Micro-MRI
- ESEM

1. Introduction

Wood is a natural, multi-scale, complex and anisotropic porous material describable as a solid polymeric matrix with pore sizes between 0-400 microns [1]. Specifically, each wooden species has structures (vessels, tracheids, fibers, pits, perforations) [2, 3] with peculiar dimensions (Fig. 1 [4]). These structures vary according to softwood (characterized by tracheids) or hardwood (characterized by vessels) classification and to the anatomical direction observed [5]. Differently from the simple anatomy of softwoods, hardwoods have more complex anatomical features and greater structural variation. By sectioning wood in the same direction of the grain (i.e. parallel to tracheids/vessels), radial parenchyma and pits with a spherical geometry and a diameter from 0 to 20 μm [2, 3] can be recognized. Pits are particularly important because allow fluids movement in the direction perpendicular to the wood grain connecting adjacent vessels or tracheids (Fig. 1) [6,7]. In the longitudinal section the macroscopic length of vessels, tracheids and fibers is also observable. In the transversal section, hardwood shows the cross section of fibres, vessels and perforation plates, all with a quite spherical geometry. Fibres have a diameter ranging from 0 to about 100 μm. Vessels are characterized by variable diameters from few microns to about 400 μm. Since vessels look like little pipelines that come from the superimposition of several cells, in some cases the cellular membrane between two adjacent cells could not be completely reabsorbed and the result is a perforation plate (Fig. 1, simple, scalariform or foraminate) that could hinder fluid movement along longitudinal direction [2]. In the same transversal view, softwood has similar structures but instead of vessels there are tracheids with a square-like cross section of size from few microns to about 60 microns [3], not including the few larger and spherical resin canals. Sometimes, both for

softwood and hardwood the presence of different substances (gums, extractives, resins, silica bodies) could determine the partial or total obstruction of pores and therefore, the reduction of fluid flow through them [8].

Despite the fact that wood is an extremely important natural resource and it is a porous hygroscopic material that can be further filled with different liquids (archaeologically excavated wood generally is waterlogged wood with very high moisture content), there are only a few papers in the literature about NMR applications to study structural features of wood species. However, in some contexts such as archaeologically excavated waterlogged wood, a rapid investigation at the microstructural level to obtain the best treatment with preservative agents is highly desirable.

On the other hand, there are numerous NMR applications for investigating porous materials, such as rocks, mortars, cements filled with liquids (usually water) [9-15]. Among NMR techniques, translational self-diffusion measurement of a fluid absorbed in a solid matrix is a powerful tool widely used in porous materials characterization [16-19]. The importance of NMR self-diffusion techniques lies in the fact that biological water in live materials is an endogenous molecular probe and its diffusion reflects tissue configuration at a microscopic level. In particular, diffusion NMR can measure water proton displacements by probing molecules motion on micrometer length scale which represents the intrinsic resolution of NMR diffusion investigations.

Through pulse field gradient (PFG) acquisition sequences [20] it is possible to quantify diffusion parameters such as the diffusion coefficient (D) and the tortuosity (τ) of water diffusing in media, that allow extrapolating information about the micro and meso-structure of the investigated samples. Indeed, water diffusing in a heterogeneous porous system can be obstructed, hindered, restricted in pores and these diffusion modalities

affect the PFG signal behavior. Using appropriate diffusion theory and models [16, 17, 19] describing the diffusion weighted NMR signal, it is possible to extract useful diffusion parameters to deduce geometric complexity, organization, orientation and size of porous system microstructure. However, diffusion NMR is intrinsically limited since it is an indirect measure of tissue microstructure and relies on inferences from models and estimation of relevant parameters. Therefore, it is necessary to validate the information obtained from NMR diffusion parameters estimated by biophysical models through complementary techniques and histology [21].

In this regard, previous works [22-25] showed the potential of diffusion measurements to determine the full pore/cells size distribution of softwood species comparing NMR results with scanning electron microscopy (SEM), optical imaging or using optical microscopy images already reported in the literature [2, 3].

Due to the growing interest in wood and its microscopic features, the aim of this work was to investigate macro- and microscopic characteristics of different wood samples by diffusion NMR techniques validated with complementary investigations. Toward this goal, the wood structures of four hardwoods and one softwood species are studied by using pulse gradient stimulated echo (PGSTE) acquisitions in fully water imbibed samples. The diffusion coefficients D, the anisotropy (a_n) and the tortuosity (τ) of water diffusing in two orthogonal directions of wood (along and perpendicular to the wood grain) together with the ranges of the pores size and their abundance were quantified for each wood sample. Results were compared and validated by micro-imaging NMR (μ-MRI), environmental scanning electron microscope (ESEM) images, density measurement (in kg/m^3), longitudinal relaxation times and imbibition times of all the wood samples. In this paper we used ESEM to in deep observe pores dimension and

pores wall structure and μ-MRI to characterize the whole sample spatial distribution of macro- and microstructures accessible with imaging with an in-plane resolution of 20 x 20 μm^2.

2. Materials and methods

2.1 Wood samples

According to the NMR spectrometer probe bore size, small sticks from five blocks of different wooden species were shaped obtaining five cylinders-like samples of about 1.5 cm in height and 0.6 cm in diameter. The cut was made so that the height of the cylinder was parallel to the wood grain. The botanical species was known as silver fir (*Abies Alba*) that is a softwood, african walnut (*Lovoa Trichilioides*), sapele mahogany (*Entandrophragma Cylindricum*), white poplar (*Populus Alba*), tanganyika walnut (*Aningeria Altissima*) that are hardwoods. The scientific denomination of each wood is based on the literature [26-28]. In order to measure wood density and imbibition times, from each wood a parallelepiped of volume of about 400 mm^3 was cut.

To perform NMR experiments each sample was boiled in distilled water until the saturation was reached. This method was adopted in order to reduce to a few minutes the total imbibition time, i.e. the total time that each wood sample required to reach the water saturation. Each sample was wrapped in parafilm and inserted without water into a 10 mm NMR tube to carry out relaxation times and diffusion experiments, whereas samples were inserted in NMR tubes and water to perform μ-MRI measurements. Once the wood samples were inserted into the magnetic field, their longitudinal direction (i.e. that one parallel to the grain) was parallel to the direction of the static magnetic field, conventionally the z direction (Fig. 1).

In order to acquire ESEM (environmental SEM) images [29], small fragments from the same five wooden blocks were cut. Unlike the traditional SEM, in which the samples need to be dehydrated and coated with a conductive layer (gold), no further preparation was required and the samples were imaged in their natural state.

2.2. Theoretical background

When an ensemble of non-interacting molecules in a fluid is followed in time in an isotropic homogeneous medium, the root mean square distance travelled, l_D (or diffusion length) increases with time as long as no boundaries are encountered, according to the Einstein relation: $l_D=(2nDt)^{1/2}$ where $n= 1,2,3$ is the space dimension and D is the bulk diffusion coefficient that can be defined as a constant and measured by a pulse field gradient (PFG) sequence [16]. Therefore, l_D represents the intrinsic resolution or the length scale with which investigating samples that contain diffusing water molecules [30]. By varying the magnetic-field gradient strength g, at a fixed diffusion time $t=\Delta$ (where Δ is the delay time between the two gradient pulses, i.e. the time window within the diffusion occurs) and fixed pulse gradient duration δ such that $\delta<<\Delta$, the NMR-signal amplitude S(g) is given by [18, 31]:

$$S(g)= S(0) \exp(-\gamma^2 g^2 \delta^2 D (\Delta - \delta/3)) \quad (1)$$

where γ is the gyromagnetic ratio of protons, $b=\gamma^2g^2\delta^2(\Delta - \delta/3)$ is the so called b-value, D is the diffusion coefficient obtained at a specific diffusion time Δ and S(0) is the signal at magnetic field gradient strength g=0.

Geometrical restrictions of the medium such as barriers and traps lead to a $D(t=\Delta)$ that decreases with time Δ. By studying the behavior of $D(\Delta)$ in a heterogeneous porous

system, it is possible to derive useful information about pores size, pores interconnection and membrane permeability [20]. In the short Δ limit, D depends linearly on $\Delta^{1/2}$ and the slope of this dependence is determined by the surface-to-volume ratio (S/V) of the water-containing compartments, irrespective of whether these compartments are connected or disconnected [20] according to the equation:

$$\frac{D(\Delta)}{D_0} = 1 - \frac{S}{V}\frac{4}{9\sqrt{\pi}}\sqrt{D_0\Delta} \quad (2)$$

On the other hand, in the limit of long Δ (i.e. $\Delta >> L^2/D_0$, where L^2 is the characteristic distance within the volume element of the porous space) and impermeable wall, the water diffusion coefficient varies according to:

$$D(\Delta)=L^2/2\Delta \quad (3)$$

Equation (3) indicates that L^2 the maximum value of l_D to be travelled in the pore confinement (i.e. the mean pore diameter), can be obtained from the slope of D vs Δ^{-1}. However, deviation from dependence of Eq. (3) can occur for semi-permeable walls [32, 33]. For materials with interconnected pores, at very long times D(Δ) approaches an asymptotic value D_∞ that is independent of the measurement time Δ, and directly related to the tortuosity τ of the porous material:

$$\tau = \frac{D_0}{D_\infty} \quad (4)$$

Tortuosity is an intrinsic property of a porous material usually defined as the ratio of actual flow path length to the straight distance between the ends of the flow path and τ of the porous system reflects the connectivity degree of the porous network [34-36].

2.3 Methods

2.3.1 Wood density and imbibition time measurement

Average dried weight values by gravimetric method were obtained for each wood species. Samples were dried inside the Universal Memmert Oven stove at the temperature of T = (103.5 ± 0.5) °C for 24 hours. Masses of each wood sample were measured with an analytical balance BP211D Sartorius and volume were calculated. Then density of each sample was obtained in kg/m^3. Furthermore, each parallelepiped of wood was also used to evaluate the imbibition time in water at T=80 ± 10 °C.

2.3.2 ESEM imaging

Electron microscopy images were collected using a Zeiss EVO LS10 Environmental Scanning Electron Microscope (ESEM) with EDS. To obtain cross-sectional images of wood the operation mode chosen was low vacuum. The vapor pressure within the chamber was of 40 Pa. The working distance (WD) ranged from 4.5 to 5.0 mm. The electron high tension was equal to 20.00 kV. The magnifications used were 300x and 1000x.

2.3.3 Micro-imaging, longitudinal relaxation times and diffusion measurements

All μ-MRI, relaxation times and diffusion experiments were performed using a Bruker Avance-400 spectrometer operating at 9.4 T with a 10 mm micro-imaging probe equipped with high performance and high strength magnetic field gradient unit characterized by a maximum gradient strength of 1200 mT/m and a rise time of 100 μs. XWINNMR® and ParaVision® 3.2 software were employed for data acquisition.

In a first step, T_1 of each sample was measured at room temperature in no-imaging modality by using Inversion Recovery (IR) sequence. The IR delays were exponentially increased from 1 ms to 6 s in 38 steps, the repetition time TR=6s and the number of averaged signals (NSA) was 4.

In a second step, knowing the longitudinal relaxation times of each species, transversal-view T_2-weighted images characterized by approximately 20x20 μm^2 in-plane resolution were acquired using the Multi Slice Multi Echo (MSME) sequence with acquisition parameters optimized for each wood species to highlight vessels and tracheids cross-section, as reported in Table 1. However, comparing acquisition parameters in Table 1 with T1 measurement reported in Table2, MSME images are not pure T2-weighted images due to the presence of an additional T1 weighted.

A Pulse Gradient Stimulated Echo sequence (PGSTE) was used to investigate water diffusion in each water-saturated wood sample. The PGSTE signal for each diffusion time (Δ) was obtained using TR=6 s, TE=1.9 ms, diffusion gradient pulse (δ)=3 ms, 32 values of b obtained with magnetic field gradient strength (g) linearly increased in 32 steps from 2% to 95% of the maximum gradient strength corresponding to 1200 mT/m and NSA=32. The b-value spanned from a minimum of 16 s/mm^2 to a maximum of 9.4 x 10^5 s/mm^2. The Δ values were 40-80-120-160-200-300-400-500-600-800-1000 ms, but the maximum value of Δ used to investigate the different species of wood was selected considering their measured T_1, so that $\Delta < T_1$ [14]. The diffusion gradient g was used both in z and x direction, i.e. along and perpendicular to the wood grain, respectively. The sample temperature in each acquisition was fixed to T= 294 K (using EDTE Bruker software).

2.4 Data Processing

2.4.1 Relaxation times

To calculate T_1 relaxation times, signal intensities (S) as a function of t=IR delays were used for fitting data to the following equation:

$$S(t) = M\,(1\text{-}\exp\,(-t/T_1)) \quad (5)$$

where T_1 is the longitudinal relaxation time and M is the associated equilibrium magnetization.

The $\overline{R^2}$ (i.e. R^2 corrected for the number of the regressors) of the one-T_1-component fit (Eq. 5) compared with the $\overline{R^2}$ of the two-T_1-components fit indicated the one-component function as best choice to fit data.

2.4.2 Diffusion coefficients

To derive D coefficients and the associated magnetizations (M), mono-, bi- and three-exponential functions were fitted to signal intensities as function of b-value S(b):

$$S(b) = M_1 \exp(-bD_1) \quad (6)$$

$$S(b) = M_1 \exp(-bD_1) + M_2 \exp(-bD_2) \quad (7)$$

$$S(b) = M_1 \exp(-bD_1) + M_2 \exp(-bD_2) + M_3 \exp(-bD_3) \quad (8)$$

Where D_1, D_2 and D_3 are the different water diffusion coefficients, M_1, M_2 and M_3 are proportional to the number of spins which diffuse with D_1, D_2, D_3. Last squared algorithm was used to fit eqs. 6-8 to data, using MatLab version R2020b.

From the preliminary μ-MRI analysis of each wooden species and considering the $\overline{R^2}$ of each data fit, the number of different water diffusion compartments with their diffusion coefficients was identified. When the magnetization associated with a specific diffusion coefficient was less than 2% the corresponding diffusive compartment was not considered. Moreover, in order to compare pore diameters abundance within which the water spins diffuse and ESEM pores diameter frequency, a correction based on the pores volume was applied to NMR magnetization values M_1, M_2 and M_3 . In the case of Eq. (7) with two different diffusion compartments D_1 and D_2 associated with two magnetizations M_1 and M_2, the correction follows the relation:

$$\frac{M_1}{M_2} = \frac{V_1}{V_2}\frac{k_1}{k_2} \qquad (9)$$

Where V_1 and V_2 are the pores volumes with two different sizes and k_1 and k_2 are the pores abundance. Approximating the pores length with the sample length, the pores volumes are only a function of the pores diameter squared.

Furthermore, the anisotropy factor was defined as follows:

$$a_n = (Dz-Dx)/(Dx+Dz) \qquad (10)$$

where Dx and Dz were the diffusion coefficients along x and z axis obtained at Δ = 200ms.

2.4.3 Pores size and tortuosity calculation from diffusion

By considering the linear part of D(Δ) curve (from Δ=80 ms to Δ=400 ms), the linear fit of Eq.(3) to data was used to evaluate the pores diameters (i.e. the mean size of tracheids, vessels, fibres and parenchyma cells cross sections) in both softwood and hardwoods. In order to estimate τ, D values obtained at different Δ were normalized as D/D_0 (where D_0 is the free water diffusion coefficient equal to $2.3x10^{-9}$ m^2/s) and plotted as a function of Δ. By extrapolating the plot trend at Δ=∞, the τ values were obtained both along x and z axes using Eq. (4). In order to evaluate the correlation between imbibition times and τ, an averaged τ over the entire volume of each sample was calculated.

2.4.4 Pores size from ESEM

ESEM images were analyzed with Gwyddion, an open access software of image analysis [37]. Briefly, a mask was applied to the ESEM images in order to detect the cavities present (representing the vessel lumen) and then they were treated as particles and analysed with the proper tool present in the software to obtain their diameter.

3. Results

T_1 values are reported in Table 2 for each wood sample with the associated standard errors (SE). White poplar has the highest while silver fir the lowest value of T_1.

3.1 μ-MRI and ESEM images

In Figure 2, transversal T_2-weigthed images with different in-plane resolution, from $15x15$ μm^2 to $31x31$ μm^2, of the five different wood samples analyzed are displayed. According to Kekkonen et al. [22, 23] results the softwood reported in Fig. 2a (silver fir) is characterized by higher and lower signal intensity zones representing earlywood (yellow circle) and latewood (green circle) areas, respectively. Image contrast is due to lower T_2 values associated to smaller pores (tracheids) in latewood and higher T_2 values

associated to larger pores in earlywood. Resin channels (Fig. 2a grey arrow) that appear as large and dark circles are also visible. Early- and late-wood are not clearly distinguishable in hardwood samples with a semi-porous or diffuse-porous ring displayed in Figs. 2b, 2c, 2d, 2e where signal intensity is higher in larger vessels than in smaller ones while hypointense areas indicate more restricted water characterized by smaller T_2 values. Among the hardwoods, white poplar (Fig. 2d) shows a different and more homogeneous structure with small vessels and fibres. Moreover, Fig. 2c shows that sapele mahogany is characterized by the largest vessels and it presents three main different structural sizes. This leads to hypothesize the existence of at least three different diffusive compartments of water characterized by different diffusion coefficients. In some vessels of sapele mahogany there are inclusions of gums and extractives (Fig. 2c orange arrow). In some woods the annual ring limit is perfectly visible, such as in silver fir and white poplar (Fig. 2a, 2d). In all the hardwoods medullary rays are observable (Fig. 2 blue arrows).

ESEM images displayed in Fig. 3 and Fig.4 show pores geometry in transversal section and anatomical details on the thick wall, such as pits that are not visible in µ-MRI. Moreover, by using ESEM microscopy in some vessels extroflexions of adjacent parenchyma cells (called *tille*) [3, 8] are better recognizable (see red arrows on Fig. 3). In Fig. 3a the square geometry of silver fir tracheids is observable. This softwood has a homogeneous structure, rich in tracheids with a gradual passage from latewood to earlywood as also observed in the MR image (Fig. 2a). In Fig. 3a is also visible a resin channel with the largest diameter, about 100 µm. Figs. 3b, 3c, 3d, 3e, referred to the hardwoods structure, confirm the existence of pores with different size. Sapele mahogany (Fig. 3c), has the largest cross-section size of vessels, above 100 µm and

often full of gum (i.e. tyloses, red arrow). Sometimes, african walnut and tanganyika walnut (Fig. 3b, 3e) present *tille* (red arrows) in their vessels cavity. ESEM images in Fig. 4 show anatomical details at few micrometers. In particular, the red circles in Fig. 4 indicate the presence of pits, i.e. pores along vessels/tracheids wall. Not only the dimension of pits but also their density seems to vary among the species as suggested from qualitative observations on the ESEM images. This hypothesis seems to agree with the literature [6, 7, 27, 28] where we also found that softwoods tracheids pits were larger (around 20 μm [3]) and less abundant than hardwoods vessels pits. Specifically, according to InsideWood 2004 database [27, 28] we found that african walnut and sapele mahogany have minute (≤ 4 μm) and small (4-7 μm) pits, white poplar has medium (7-10 μm) and large (≥ 10 μm) pits and tanganyika walnut small and medium pits.

3.2 Diffusion and cross sectional vessels/tracheids size evaluation

PGSTE data were of good quality showing a signal to noise ratio SNR> 10 for the experimental points obtained at the highest b-values. The parameter $\overline{R^2}$ was closed to 1 for all the fits.

The D(Δ) behavior and the associated magnetization obtained along x and z gradient directions (Fig. 1) for the different diffusion compartments in all wood samples are shown in Figs. 5a, 5b, 5c and Figs. 6a, 6b, 6c. For each diffusion compartment (x1, x2, x3, z1, z2, z3) D(Δ) curves are differently colored for each wood sample.

According to preliminary μ-MRI and ESEM evaluation, along x gradient direction (Fig. 5) sapele mahogany and tanganyika walnut are characterized by three different diffusion compartments with diffusion values quantified by Eq. (8), while silver fir, african

walnut and white poplar show only two different diffusion with diffusion values obtained by Eq. (7). Along z direction (Fig. 6), sapele mahogany is characterized by three diffusion compartments, tanganyika walnut and african walnut by two diffusion compartments and only one diffusion compartment was highlighted for silver fir and white poplar the diffusion coefficients of which were quantified by Eq. (6).

In Table 3 for each wood samples the diffusion coefficient values quantified at Δ = 200 ms both along x and z direction (Fig. 1) and the anisotropy factor (a) obtained by Eq.(10) are shown. Silver fir is characterized by the highest anisotropy.

In Fig.7 an example of Eq. (3) fitted to diffusion data as a function of Δ^{-1} is displayed and in Table 4 pores diameter evaluated by using the linear fit of Eq.(3) and the pores abundances by using Eq.(9) are displayed.

ESEM pores frequency in transversal direction (i.e. the transversal sections of vessels) calculated for four ranges of size are resumed in Table 5.

3.3 Tortuosity and parameters correlations

Figure 8 displays Dx_1/D_0 against Δ to show how τ was calculated with the red line indicating the asymptotic value of D/D_0 at $\Delta=\infty$, while the mean τ values calculated along x and z direction are reported in Table 6.

Fig. 9 shows the correlation plots of average τ as a function of the imbibition times (Fig. 9a), the imbibition times against densities (Fig. 9b) and T_1 against the imbibition times (Fig. 9c). A significant linear correlation (with $p<0.0063$ and $r=0.97$) was found between imbibition times and average τ and between imbibition times and T_1 (with $p<0.0222$ and $r=0.93$). Conversely, no significant correlation was found between imbibition times and wood density. Finally, in Fig. 10 the graph of a_n vs mean τ along x gradient direction is displayed.

4. Discussions

According to the hierarchical structure of wood, D(t) is dependent on diffusion time t= Δ in all investigated water-soaked samples (Figs. 5 and 6). The greater the decrease of the D(Δ) curve, the greater the deviation of the water dynamics from the Gaussian diffusion [38]. As the D(Δ) decrease indicates the presence of barriers and traps to water diffusion (which cause non-Gaussian dynamics of water in wooden samples), the more the curve decreases rapidly, the more complex the porous system is. This behavior can be quantified by water τ, a measure of wood complexity whereas the diffusion anisotropy (a_n) (Tab. 3) provides differences of the wood structure when studied in different directions. This paper shows that τ and a_n extracted from the diffusion measurements, characterize different wood species better than their dry density (Tables 3 and 6 and Figs. 9 and 10) or their mean pore sizes (Tables 4 and 5). Therefore, a_n *vs* τ could be used as an alternative method to high resolution images (μ-MRI and ESEM or optical) for differentiate waterlogged wood.

As expected, due to τ dependence on hydraulic conductivity [39], averaged τ values over sample volume are significantly correlated to imbibition times of wood samples (Fig. 9). Therefore, τ and a_n may result useful parameters to describe the water flux in the direction perpendicular and parallel to the wood grain and to characterize the wood samples features. A significant correlation was also found between T_1 and the imbibition times indicating that also T_1 can be used to describe the wood structure. However, this occur in sample of modern wood soaked with pure water. T_1 values are in general influenced by the presence of paramagnetic impurities. Usually, in archaeological submerged woods different kinds of paramagnetic impurities such as

resins and extractives or depositions of salts and iron are found. Therefore, τ measurement instead of T_1 is more reliable for obtaining topological and structural information from waterlogged wood.

Regarding diffusion quantification along x direction, fast component diffusion (diffusion of about 10^{-9} m^2/s) derived from vessels/tracheids while the second slow diffusion component derived from a greater number of walls and barriers which contain more trapped water in wood parenchyma (diffusion of about 10^{-10} m^2/s). As it is possible to capture from Fig.5 in two of the five wood samples a third diffusion component was found (diffusion of about 10^{-11} m^2/s) that we attributed to water more trapped (compared to that of the second diffusion compartment) in microscopic wood structures.

In the following we will discuss compare and explain NMR diffusion results for each investigated wood species. To this end, we will highlight the agreement of the NMR results with the results obtained with complementary techniques.

4.1 Silver fir and white poplar

Silver fir is characterized by the shortest T_1 and the lowest dry density. This result is in agreement with silver fir structure composed by more pores and voids than cell walls (made of high density polymers [40]). Conversely, white poplar shows the longest T_1 but a quite low dry density (Fig.9). White poplar is composed by a smaller number of pores and voids than silver fir and a greater number of walls and barriers which contain more trapped water with a slow dynamic. We also found two main diffusion compartments in silver fir and white poplar when the diffusion gradient is perpendicular to the wood grain (Dx compartments), whereas when the diffusion gradient follows the wood grain (Dz compartments), silver fir and white poplar are characterized by only

one diffusion compartment. This is in agreement with the MR images (Fig. 2a and 2d) showing a quite homogeneous structure both for silver fir and white poplar. In fact, silver fir is a softwood [41] (Figs 2a, 3a and 4a) with a relatively simple structure: 90-95% of its cells are tracheids or fibre-tracheids. On the other hand, white poplar, despite being a hardwood, differs from the other hardwood samples investigated in this work because it is composed by only one main size of vessels that occupies around the 40% of its structure. Since the water diffuses more easily along the main axis of vessels and tracheids (z axis, see Fig. 1) than perpendicular to vessels and tracheids (x axis), this means that the water diffusion is weakly hindered along z while along x is more confined and the two diffusion compartments (for which Dx_1 and Dx_2 are quantified) are representative of different pores sizes. For silver fir, the two mean Dx values are likely related to different earlywood and latewood tracheids size, while in white poplar are related to different vessels and fibres size. According to the less pits density in softwood compared to hardwoods a_1 (Table 3) is much higher for silver fir than white poplar (34% and 22%, respectively). The ranges of the pores diameter extracted using the linear fit of Eq.(3) are in large agreement with μ-MRI and ESEM results. For silver fir, two clusters of pores with mean diameter around 16.29 ± 0.35 μm and 7.94 ± 1.16 μm can be attributed to earlywood tracheids and latewood tracheids, respectively. The pores abundance associated to the diffusion components (k parameters in Table 4) indicates that silver fir structure is composed by about 70% of earlywood tracheids and 30% of latewood tracheids, which agrees with the information provided by MR image in Fig. 2a where the earlywood occupies a greater volume than the latewood and with the ESEM frequencies (Table 5). White poplar shows vessels with a mean diameter of 21.45 ± 3.38 μm that occupy the 42% of its structure, and fibres of 10.73 ± 0.29 μm that

occupy the remaining 58%. According to the diffusion results, the tortuosity perpendicular to vessels and tracheids (τx) is higher than the tortuosity along vessels and tracheids (τz, Table 6). Silver fir and the white poplar have the same τz but different τx value which in the white poplar is the highest revealing its more complex structure probably caused both by a greater extension of parenchyma compared to vessels and fibers and to a greater dispersion of pits size [6,7]. Regarding different τ related to different diffusion compartments, in silver fir the low tortuosity τx_1 may be due to higher permeability of earlywood tracheids cell walls compared to that of latewood tracheids cell walls (high tortuosity τx_2) related to their tracheids walls thickness that is higher in latewood compared to earlywood tracheids. In white poplar, the fibres walls (high tortuosity τx_2) show a higher impermeability than the vessels walls (low tortuosity τx_1) [39, 42] which agrees with the inconspicuous pits of hardwoods fibres described by Wiedenhoeft 2012 [43]. This result also agrees with the correlation plot showed in Figs. 9a and 9c where the long imbibition time of white poplar correlates with its high tortuosity and long T_1.

Diffusion and τ (Fig.5 and Tab. 6) results can also explain some peculiar features of white poplar reported in the literature. Some authors [44] highlight that the water imbibition in poplar is not a penetration basically due to capillary effects associated with the size of the main voids, but it is strongly affected by the adsorption of confined bound water in cell walls. In particular, bound water appears to progress far beyond the front of free water in vessels, and the free water penetration along the main sample axis apparently coincides with the development of a region saturated with bound water. This can explain why water imbibition is about three orders of magnitude slower than expected from standard Washburn imbibition process [44, 45]. In agreement with these

observations, in this paper we found that imbibition time and the mean tortuosity of white poplar are longer than those of the other wood samples (Fig. 9). In particular, τx_2 obtained from D(Δ) of the slower diffusion compartment is one order of magnitude greater than that of the other woods. The higher the value of the tortuosity, the more the water makes complicated routes with deviations and local entrapment in the porous system. This is in agreement with the dynamics of imbibition in white poplar wood that appears to be mainly governed by bound water movement in the sample [44].

4.2 African walnut, tanganyika walnut and sapele mahogany

Despite the dry density is close for all the three samples, the measured T_1 value is similar for african walnut and tanganyika walnut (see Table 2) but higher for sapele mahogany.

In african walnut, diffusion along both x and z direction (Fig. 5 and 6) is described by two compartments. On the other hand, sapele mahogany and tanganyika walnut show three main compartments when diffusion gradient is along x while three and two compartments, respectively, when diffusion gradient is along z. The presence of several diffusion components indicates a heterogenous structure with three main different pores size for sapele mahogany and tanganyika walnut and two main sizes for african walnut (Table 4). The mean size d1, d2 and d3 (Tab. 4) obtained by diffusion NMR are in good agreement with sizes quantified by ESEM (Tab. 5). On the other hand, the pores of vessels large more than 40 μm are not measurable using water PGSTE with the parameters selected in this work. Indeed, the limiting length from water diffusion arises from the water T1 (Table 2) and the free diffusion coefficient D0 of about 2x10-9 m2/s giving a maximum diffusion length of (DoΔ)1/2 with Δ<T1, i.e. less than 45 μm.

Considering the limiting diffusion length from water diffusion around 45 μm [46], this work suggests the great utility of the μ-MRI for the evaluation of larger pores dimension. Unlike the ESEM exam, which allows the investigation of small portions of the wood samples, μ-MRI provides information of the whole wooden sample giving a global knowledge about microstructures distribution. By looking at the MR images and ESEM images we can notice that above 45 μm sapele mahogany has larger vessels than tanganyika and african walnut. The abundance of pores larger than 45 μm is the same for sapele mahogany and tanganyika walnut but much lower for african walnut (Table 5). Diffusion results show that sapele mahogany is composed of about 9% by pores with a mean size of 22.36 ± 1.14 μm likely associated with vessels, for the 27% by pores of 11.31 ± 0.24 μm associated with fibres and for the remaining 64% by pores of 4.13 ± 0.07 μm associated with parenchyma cells. Tanganyika walnut has the 57% of pores with a mean diameter of 20.72 ± 2.31 μm attributed to vessels, the 31% with a diameter of 9.82 ± 0.98 μm attributed to fibres and the 11% with diameter of 4.18 ± 0.32 likely associated with parenchyma cells. African walnut shows two clusters of pores around 18.01 ± 1.34 μm and 4.94 ± 0.65 μm, associated with vessels and parenchyma cells respectively, the former one occupies the 40% and the latter the 60% of the structure. The anisotropic diffusion behavior is observed in all the three samples (Table 3) where tanganyika walnut and african walnut are characterized by a similar mean anisotropy while sapele mahogany shows a lower a_n. This is explained by the presence of perforation plate, tille and tyloses in sapele mahogany (Fig. 3c) that cause hindered diffusion also along z direction reducing diffusion coefficient Dz (Table 3).

In the three samples, average tortuosity along x is higher than the tortuosity along z confirming the presence of more hindered water along the x axis (i.e. perpendicular to

vessels). The average tortuosity is higher for sapele mahogany compared to tanganyika walnut and african walnut, indicating a more complex structure for the former one. Tanganyika walnut, despite having T_1, imbibition time and a_n similar to african walnut, shows a slightly greater tortuosity in agreement with a description of tanganyka walnut characterized by three main diffusion compartments compared to the two compartments of african walnut.

5. Conclusions

The physical and mechanical properties of wood are mainly determined by their structure. In this paper we have investigated wood structural properties in water imbibed wood samples by diffusion NMR and complementary techniques to validate diffusion results. This work suggests that NMR non-destructive time dependent diffusion D(t) investigations can be useful to explore wood structure topology and morphology. Among parameters evaluated by water D(t) measurement, the tortuosity correlated to diffusion anisotropy rather than the estimated mean pore sizes can identifies and characterize the different species of softwood and hardwood here investigated. Importantly, the combined use of PGSTE NMR and micro-MRI expands the scale of the dimensions observable by water NMR in wood samples covering all the interesting length scales of wood structure, from large cross-section of vessels, tracheids and resin canals well visible by transversal-view MRI to fibres, parenchyma and small pits of tracheids and vessels whose dimensions are only indirectly quantifiable through NMR diffusion measurements. The proposed study could represents a powerful protocol applicable for non-destructive diagnostics and investigation of the conservation state waterlogged archaeological wood which is naturally full of water and that usually need to have a rapid investigation at the microstructural level to obtain the best treatment

with preservative agents [47]. Since the method shown and validated here is based on the acquisition of the diffusion weighted signal in non-imaging modality, it can be implemented and used on portable NMR spectrometers for in situ monitoring of waterlogged archaeological wood [48].

Acknowledgment

We acknowledge funding of Regione Lazio under the ADAMO project n. B86C18001220002 of the Centre of Excellence at the Technological District for Cultural Heritage of Lazio (DTC) and "Torno Subito" Operational Program European Social Fund Lazio Region POR 2014-2020.

Competing Interests statement

The authors declare no competing financial interest.

AUTHORSHIP STATEMENT

I, Silvia Capuani, as corresponding author, with the approval of all authors declare that:

All individuals who met the authorship criteria are listed as authors and all authors certify that they have participated sufficiently in the work to take public responsibility for the content, including participation in the concept, design, analysis, writing or revision of the manuscript.

Furthermore, as the corresponding author I certify that:

the material or similar material reported in the manuscript has not been and will not be posted or published in any other journal prior to its appearance in Magnetic Resonance Imaging

References

[1] Plötze M, Niemz P. Porosity and pore size distribution of different wood types as determined by mercury intrusion porosimetry. Eur J Wood Prod 2011; 69:649-657. https://doi.org/10.1007/s00107-010-0504-0

[2] Wheeler EA, Baas P, Gasson PE. Iawa list of microscopic features

for hardwood identification. 4th printing. Leiden: 2007.

[3] Richter HG, Grosser D, Heinz I, Gasson PE. Iawa list of microscopic features for softwood identification. IAWA J 2004; 25:1–70. https://doi.org/10.1163/22941932-90000349

[4] Encyclopædia Britannica. https://www.britannica.com/plant/tree/The-anatomy-and-organization-of-wood#/media/1/603935/55253, 2020. (accessed 16 March 2020).

[5] Capuani S, Stagno V, Missori M, Sadori L, Longo S. High resolution Multiparametric MRI of Contemporary and Waterlogged Archaeological Wood. Magn Reson Chem 2020; 65:1-10. http://dx.doi.org/10.1155/2015/948610

[6] Choat B, Cobb AR, Jansen S. Structure and function of bordered pits: new discoveries and impacts on whole-plant hydraulic function. New Phytol 2008; 177:608-626. https://doi.org/10.1111/j.1469-8137.2007.02317.x

[7] Jones HG. Plants and microclimate, a quantitative approach to environmental plant physiology. 3rd edition. Cambridge: Cambridge University Press; 2014.

[8] Kettunen PO. Wood Structure and Properties. Uetikon-Zuerich: Trans Tech Publications, Ltd; 2006.

[9] Kleinberg RL, Kenyon WE, Mitra PP. Mechanism of NMR Relaxation of Fluids in Rock. J Magn Reson, Series A 1994; 108:206-214. https://doi.org/10.1006/jmra.1994.1112

[10] Fordham EJ, Sezginer A, Hall LD. Imaging Multiexponential Relaxation in the (y, Log_eT_1) Plane, with Application to Clay Filtration in Rock Cores. J Magn Reson, Series A 1995; 113:139-150. https://doi.org/10.1006/jmra.1995.1073

[11] Mitchell J, Souza A, Fordham E, Boyd A. A finite element approach to forward modeling of nuclear magnetic resonance measurements in coupled pore systems. J Chem Phys 2019; 150:e154708. https://doi.org/10.1063/1.5092159

[12] Alesiani M, Capuani S, Maraviglia B. NMR applications to low porosity carbonate stones. Magn Reson Imaging 2003; 21:799-804. https://doi.org/10.1016/S0730-725X(03)00099-7

[13] Alesiani M, Capuani S, Maraviglia B, Giorgi R, Baglioni P. Effects induced on marbles by water-repellent compounds: the NMR contribution. Appl Magn Reson 2002; 23: 63-73. https://doi.org/10.1007/BF03166184

[14] Faux DA, McDonald PJ. Nuclear-magnetic-resonance relaxation rates for fluid confined to closed, channel, or planar pores. Phy. Rev E 2018; 98(6):1 – 14. https://doi.org/10.1103/PhysRevE.98.063110

[15] Gladden LF, Mitchell J. Measuring adsorption, diffusion and flow in chemical engineering: applications of magnetic resonance to porous media. New J Phys 2011; 13:e035001. https://doi.org/10.1088/1367-2630/13/3/035001

[16] Callaghan PT. Principles of Nuclear Magnetic Resonance Microscopy. New York: Oxford University Press Inc; 1991.

[17] Price WS. NMR studies of translational motion: principles and applications. Leiden: Cambridge University Press, 2009.

[18] Stejskal EO, Tanner JE. Spin Diffusion Measurements: Spin Echoes in the Presence of a Time Dependent Field Gradient. J Chem Phys 1965; 42:288-292. https://doi.org/10.1063/1.1695690

[19] Callaghan PT, Coy A, Macgowan D, Packer KJ, Zelaya FO. Diffraction-like effects in NMR diffusion studies of fluids in porous solids. Nature 1991; 351:467-469. https://doi.org/10.1038/351467a0

[20] Sen PN. Time-Dependent Diffusion Coefficient as a Probe of Geometry. Concepts Magn Reson 2004; 23A:1-21. https://doi.org/10.1002/cmr.a.20017

[21] Jelescu IO, Budde MD. Design and Validation of Diffusion MRI Models of White Matter. Front Phys 2017; 5:61. https://doi.org/10.3389/fphy.2017.00061

[22] Kekkonen PM, Telkki V-V, Jokisaari J. Determining the Highly Anisotropic Cell Structures of Pinus *sylvestris* in Three Orthogonal Directions by PGSTE NMR of Absorbed Water and Methane. J Phys Chem B 2009; 113:1080-1084. https://doi.org/10.1021/jp807848d

[23] Kekkonen PM, Telkki V-V, Jokisaari J. Effect of Thermal Modification on Wood Cell Structures Observed by Pulsed-Field-Gradient Stimulated-Echo NMR. J Phys Chem C 2010; 114:18693-18697. https://doi.org/10.1021/jp1060304

[24] Johannessen EH, Hansen EW, Rosenholm JB. Fluid Self-Diffusion in Scots Pine Sapwood Tracheid Cells. J Phys Chem B 2006; 110:2427-2434. https://doi.org/10.1021/jp0556431

[25] Wycoff W, Pickup S, Cutter B, Miller W, Wong TC. The Determination of the Cell Size in Wood by Nuclear Magnetic Resonance Diffusion Techniques. Wood Fiber Sci 2007; 32:72-80.

[26] Wood anatomy of central European Species. http://www.woodanatomy.ch , 2020 (accessed 28 February 2020).

[27] InsideWood. 2004-onwards. http://insidewood.lib.ncsu.edu/search, 2020 (accessed 28 February 2020).

[28] Wheeler EA. InsideWood - a web resource for hardwood anatomy. IAWA J 2011; 32 (2):199-211.

[29] Turkulin H, Holzer L, Richter K, Sell J. Application of the ESEM technique in wood research: part I. Optimization of imaging parameters and working conditions. Wood Fiber Sci, 2005; 37:552-564. Retrieved from https://wfs.swst.org/index.php/wfs/article/view/246.

[30] Capuani S, Manenti G, Iundusi R, Tarantino U. Focus on Diffusion MR Investigations of Musculoskeletal Tissue to Improve Osteoporosis Diagnosis: A Brief Practical Review. BioMed Res Int 2015; 1-10:948610. http://dx.doi.org/10.1155/2015/948610

[31] Norris DG. The effects of microscopic tissue parameters on the diffusion weighted magnetic resonance imaging experiment. NMR Biomed 2001; 14:77–93. https://doi.org/10.1002/nbm.682

[32] Anisimov AV, Sorokina NY, Dautova NR. Water diffusion in biological porous systems: a NMR approach. Magn Reson Imaging 1998; 16:565–568. https://doi.org/10.1016/S0730-725X(98)00053-8

[33] Valiullin R, Skirda V. Time dependent self-diffusion coefficient of molecules in porous media. J Chem Phys 2001; 114:452–458. https://doi.org/10.1063/1.1328416

[34] Dullien FAL. Porous Media: Fluid Transport and Pore Structure. New York: Academic Press; 1979.

[35] Mitra PP, Sen PN, Schwartz LM, Ledoussal P. Diffusion Propagator as a Probe of the Structure of Porous Media. Phys Rev Lett 1992; 68.3555–3558. https://doi.org/10.1103/PhysRevLett.68.3555

[36] Zecca M, Vogt SJ, Connolly PR, May EF, Johns ML. NMR Measurements of Tortuosity in Partially Saturated Porous Media. Transport Porous Med 2018; 125:271-288. https://doi.org/10.1007/s11242-018-1118-y

[37] Nečas D, Klapetek P. Gwyddion: an open-source software for SPM data

Analysis. Cent Eur J Phys 2012; 10:181–188. https://doi.org/10.2478/s11534-011-0096-2

[38] Kiselev VG. Fundamentals of diffusion MRI physics. NMR Biomed 2017; 30:e3602. https://doi.org/10.1002/nbm.3602

[39] Ghanbarian B, Hunt AG, Ewing RP, Sahimi M. Tortuosity in Porous Media: A Critical Review. Soil Sci Soc Am J 2013; 77:1461-1477. https://doi.org/10.2136/sssaj2012.0435

[40] Alesiani M, Proietti F, Capuani S, Paci M, Fioravanti M, Maraviglia B. ^{13}C CPMAS NMR Spectroscopic Analysis Applied to Wood Characterization. Appl Magn Reson 2005; 29:177-184. https://doi.org/10.1007/BF03167005

[41] Schultze-Dewitz G, Götze H. Transverse dimensions of softwood tracheids. Feddes Repert 1992; 103:195-204. https://doi.org/10.1002/fedr.19921030307

[42] Fengel DI, Wegener G. Wood-Chemistry, ultrastructure, reactions. Remagen: Verlag Kessel; 2003.

[43] Wiedenhoeft AC. Structure and Function of Wood. In: Rowell RM, editors. Handbook of wood chemistry and wood composites, 2nd edition, Boca Raton: CRC Press; 2012, p 9-32.

[44] Hamraoui A, Nylander T. Analytical Approach for the Lucas–Washburn Equation, J Colloid Interface Sci 2002; 250:415-21. https://doi.org/10.1006/jcis.2002.8288

[45] Zhou M, Caré S, Courtier-Murias D, Faure P, Rodts S, Coussot P. Magnetic resonance imaging evidences of the impact of water sorption on hardwood capillary imbibition dynamics. Wood Sci Technol 2018; 52:929–955. https://doi.org/10.1007/s00226-018-1017-y

[46] Mair RW, Hurlimann MD, Sen PN, Schwartz LM, Patz S, Walsworth RL. Tortuosity measurement and the effects of finite pulse widths on xenon gas diffusion NMR studies of porous media. Magn Reson Imaging 2001; 19:345–351. https://doi.org/10.1016/S0730-725X(01)00247-8

[47] Kanazawa Y, Yamada T, Kido A, Fujimoto K, Takakura K, Hayashi H, Fushimi Y, Kozawa S, Koizumi K, Okuni M, Ueda N, Togashi K. Internal evaluation of impregnation treatment of waterlogged wood; relation between concentration of internal materials and relaxation time using magnetic resonance imaging. Magn Reson Imaging 2017; 38:196-201. http://dx.doi.org/10.1016/j.mri.2017.01.010.

[48] Stagno V, Mailhiot S, Capuani S, Galotta G, Telkki VV. Testing 1D and 2D single-sided NMR on Roman age waterlogged woods. Journal of Cultural Heritage, 2021, Available on line 24 June 2021, https://doi.org/10.1016/j.culher.2021.06.001.

Figure 1. Sketch of the 3D wood structure in tangential, radial and longitudinal view to highlight the main porous elements of both softwood and hardwood where water molecules diffuse (adapted from Encyclopædia Britannica, 2020 [4]). In figure the x and z axis are also indicated.

Figure 2. Transversal view T_2-weighted images of a) silver fir with in plane resolution R = 15 x 15 μm^2 and where green circle indicates the late wood and yellow circle the early wood; b) african walnut with R = 31 x 31 μm^2; c) sapele mahogany with R = 27 x 27 μm^2; d) white poplar with R = 18 x 18 μm^2; e) tanganyika walnut with R = 25 x 25 μm^2. Red arrows indicate the annual ring limit; white arrow the resin canal; blue arrows the rays; orange arrow the presence of tyloses in vessels. The acquisition parameters are reported in Table 1.

Figure 3. Transversal view ESEM images of a) silver fir; b) african walnut; c) sapele mahogany; d) white poplar; e) tanganyika walnut. Images were acquired with a 300 X magnification. The scale bar is 100 µm. Red arrows indicate the presence of *tille* or tyloses in vessels; black arrow shows the resin canal of the softwood.

Figure 4. 1000 X magnification ESEM images displayed to highlight anatomical details such as pits and pores walls (see red circles) of a) silver fir; b) african walnut; c) sapele mahogany; d) white poplar; e) tanganyika walnut. The scale bar is 10 µm.

Figure 5. Behavior of the three components of diffusion coefficient (a, b, c) and the associated magnetizations (d, e, f) as a function of t=Δ obtained using gradient strength g along x direction (i.e. perpendicular to the wood grain). Points show experimental data. The connecting lines are for illustration purpose only. The D(Δ) behavior suggest non-Gaussian diffusion behaviour of water in waterlogged wood in each of the three diffusion compartments 1,2 and 3. Note that the average diffusion value in the three

compartments differs by an order of magnitude (is about 10^{-9} m^2 / s in the first compartment attributed to the bulk water in the vessels and tracheids, is about 10^{-10} m^2/s in the second compartment defined by the cells and membranes of the parenchyma and is about 10^{-11} m^2/s in the third diffusive compartment that we find only in the parenchyma of the tanganyika walnut and in the sapele mahogany.

Figure 6. Behavior of the three components of diffusion coefficient (a, b, c) and the associated magnetizations (d, e, f) as a function of Δ obtained using gradient strength g along z direction (i.e. parallel to the wood grain). Points show experimental data. The connecting lines are for illustration purpose only.

Figure 7. a) An example of Dx_1 behavior as a function of Δ with the red zone indicating data used to perform the fit with Eq. (3). b) the result obtained by fitting Eq. (3) to Dx_1 vs. $2\Delta^{-1}$ data. The more the decay differs from the linearity and the more the cell walls are permeable. Plots refer to sapele mahogany sample.

Figure 8. Plot of Dx_1/D_0 against Δ to show the different behavior of D(t) among different wood species and how tortuosity was calculated. The red line indicates the asymptotic value of D/D_0 at $\Delta=\infty$.

Figure 9. Correlation plots of a) average tortuosity vs. imbibition time; b) imbibition time vs. dry density; c) T_1 vs. imbibition time. The linear correlation r and the correlation significance p are also displayed for each graph.

Figure 10. Anisotropy (a_n) vs mean tortuosity along x-direction (τ_x) graph. Using this graph it is possible to distinguish well the different wood species. Evaluation of a_n and τ could be an alternative method to differentiate wood species of waterlogged wood when high resolution images (μ-MRI and ESEM) are not available.

Table 1. Acquisition parameters for T_2-weighted μ-MRI.

Species	Sequence	TE/TR (ms)	NSA*	Number of Slices	Slice Thickness (μm)	FOV* (cm^2)	MTX* (pixels)	In-plane resolution (μm^2)
Silver Fir	MSME	6.2/800	128	8	250	0.75x0.75	512x512	15x15
African Walnut	MSME	4.4/900	256	10	200	0.80x0.80	256x256	31x31
Sapele Mahogany	MSME	3.0/1600	256	8	250	0.70x0.70	256x256	27x27
White Poplar	MSME	6.0/2000	128	8	300	0.90x0.90	512x512	18x18
Tanganyika Walnut	MSME	3.8/900	256	10	200	0.65x0.65	256x256	25x25

*NSA=number of signal averages; FOV=Field of view; MTX=matrix dimension.

Table 2. T_1 values obtained using a mono-component T_1 model with the standard errors (SE)

Species	$T_1 \pm$ SE (ms)
Silver Fir	413 ± 14
African Walnut	512 ± 28
Sapele Mahogany	1231 ± 14
White Poplar	1756 ± 11
Tanganyika Walnut	502 ± 21

Table 3. Diffusion coefficients values in m^2/s measured along x and z direction considering both the first and the second diffusion compartments found in all wood samples and the diffusion anisotropy (a_n) in percentage calculated at Δ= 200ms considering the first diffusion compartment (Dx1 and Dz1).

	Dz_1 ($x10^{-9}$ m^2/s)	Dx_1 ($x10^{-9}$ m^2/s)	a_n	Dz_2 ($x10^{-10}$ m^2/s)	Dx_2 ($x10^{-10}$ m^2/s)
Silver Fir	1.58 ± 0.03	0.75 ± 0.04	36 %	-	2.19 ± 0.17
African Walnut	1.70 ± 0.02	1.21 ± 0.03	17 %	1.40 ± 0.08	0.97 ± 0.09
Sapele Mahogany	1.51 ± 0.02	1.26 ± 0.03	9%	1.94 ± 0.16	1.26 ± 0.09
White Poplar	1.70 ± 0.02	1.08 ± 0.04	22 %	-	1.02 ± 0.06
Tanganyika Walnut	1.76 ± 0.02	1.23 ± 0.02	18 %	1.50 ± 0.09	1.27 ± 0.04

Table 4. Pores diameter and standard errors obtained by the linear fit of Eq.(3) together with pores abundances obtained by Eq.(9) from the diffusion measurements.

Species	d1 (μm)	d2 (μm)	d3 (μm)	k_1 (%)	k_2 (%)	k_3 (%)
Silver Fir	16.29 ± 0.35	7.9 ± 1.16	-	70	30	-
African Walnut	18.01 ± 1.34	4.94 ± 0.65	-	40	60	-
Sapele Mahogany	22.36 ± 1.14	11.31 ± 0.24	4.13 ± 0.07	43	32	25
White Poplar	21.45 ± 3.58	10.73 ± 0.29	-	42	58	-
Tanganyika Walnut	20.72 ± 2.31	9.82 ± 0.98	4.18 ± 0.32	57	31	11

Table 5. ESEM pores frequency divided in four size ranges: 0-4 μm, 5-12 μm, 13-45 μm and > 45 μm.

Species	f0 (%) > 45 μm	f1(%) 13 - 45 μm	f2 (%) 5 - 12 μm	f3 (%) 0 - 4 μm
Silver Fir	2	87	11	0
African Walnut	1	29	59	11
Sapele Mahogany	3	31	62	5
White Poplar	5	42	51	2

Tanganyika Walnut	3	20	61	17

Table 6. Wood tortuosity (τ) along x and z obtained by Eq.(4) from the first two diffusion compartments and their weighted average over each sample volume

Species	τx_1	τx_2	τz_1	τz_2	average τx	average τz
Silver Fir	3.49 ± 0.14	10.80 ± 1.39	1.70 ± 0.04	-	2.70 ± 0.23	1.70 ± 0.04
African Walnut	2.48 ± 0.09	36.41 ± 0.99	1.45 ± 0.01	23.20 ± 0.80	2.88 ± 0.09	1.92 ± 0.05
Sapele Mahogany	3.07 ± 0.21	30.83 ± 0.54	1.89 ± 0.08	15.52 ± 0.0	5.05 ± 0.14	2.03 ± 0.04
White Poplar	7.87 ± 0.53	102.44 ± 6.05	1.70 ± 0.0	.	13.86 ± 0.84	1.70 ± 0.04
Tanganyika Walnut	2.52 ± 0.18	30.26 ± 0.34	1.39 ± 0.0	23.80 ± 0.79	4.00 ± 0.72	2.60 ± 0.08

Graphical abstract

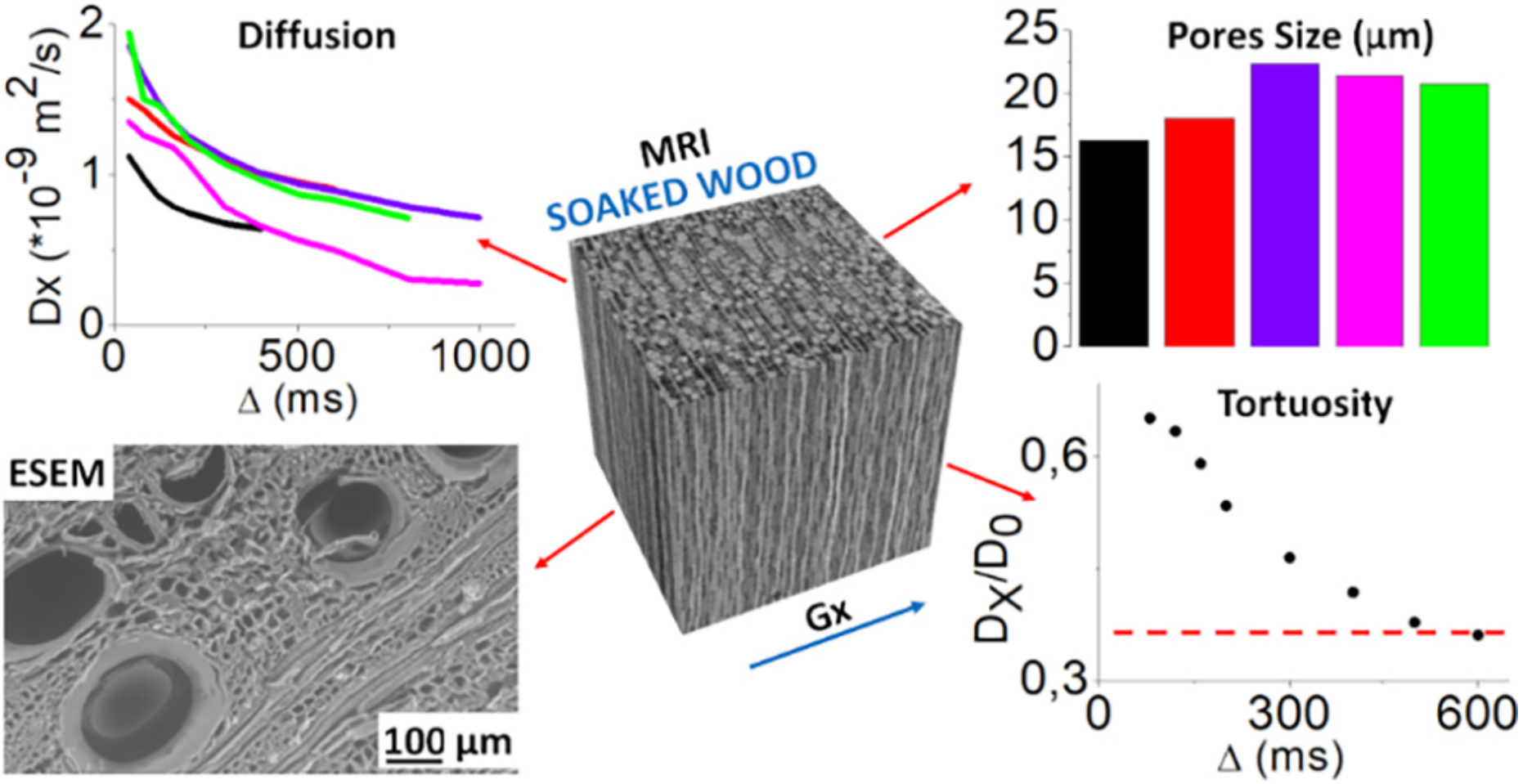

Graphics Abstract

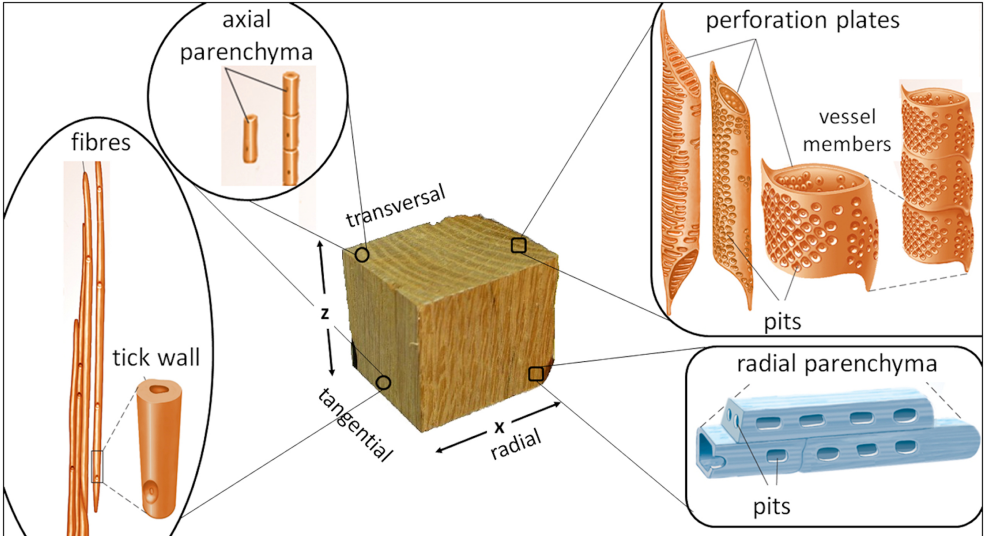
axial
parenchyma
fibres
tick wall
transversal
z
tangential
x
radial
perforation plates
vessel
members
pits
radial parenchyma
pits

Figure 1

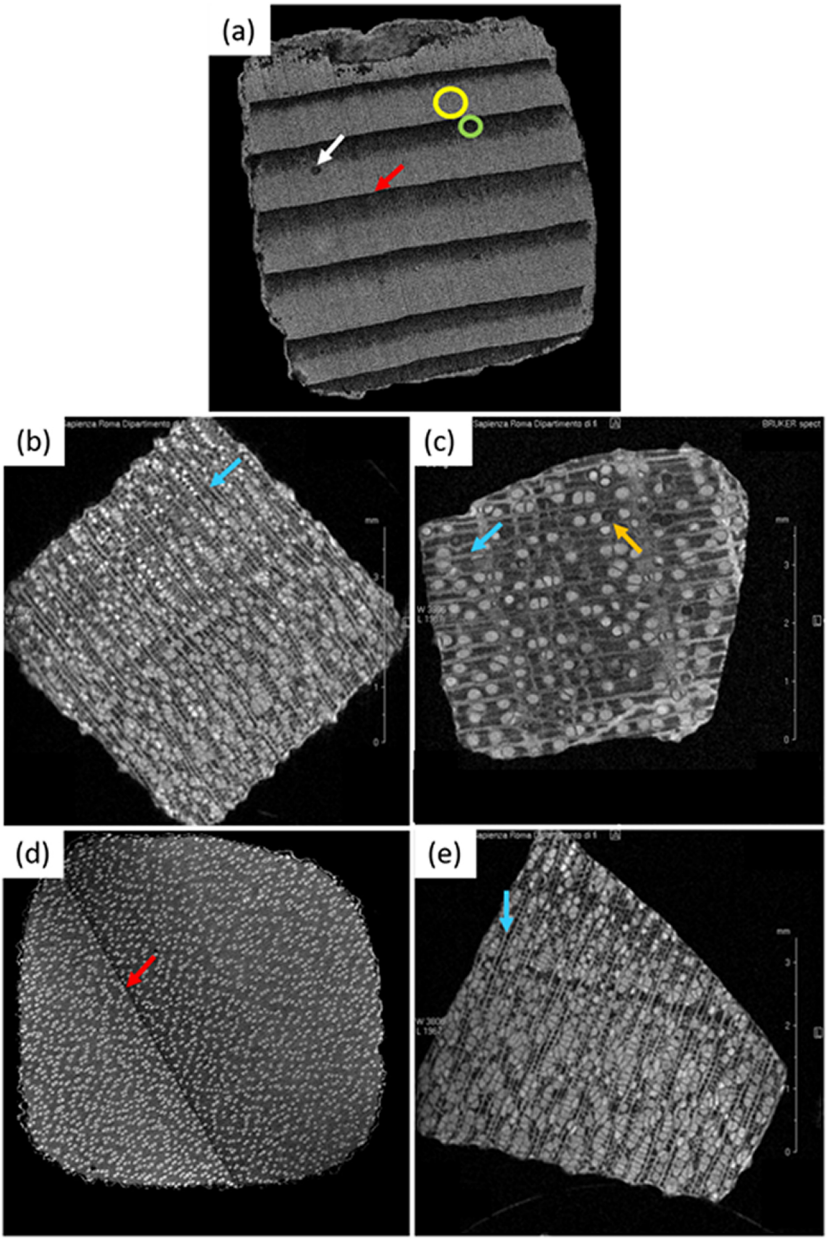

Figure 2

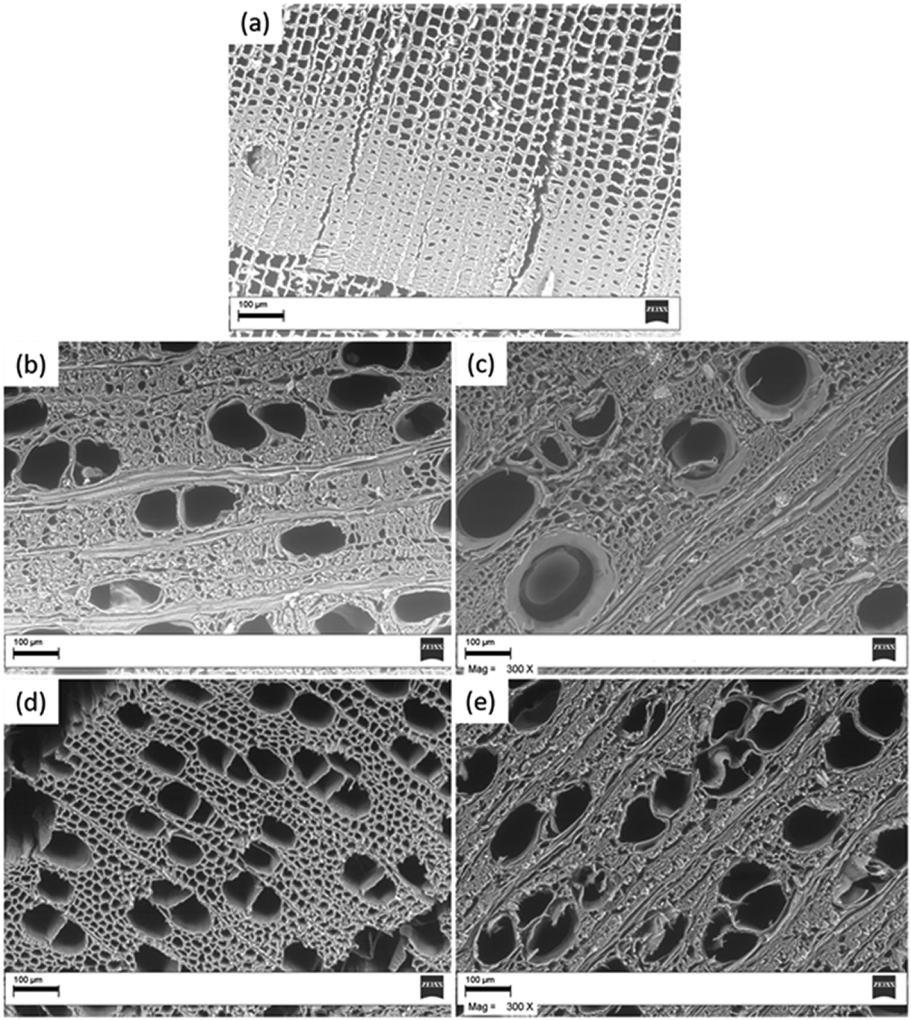

Figure 3

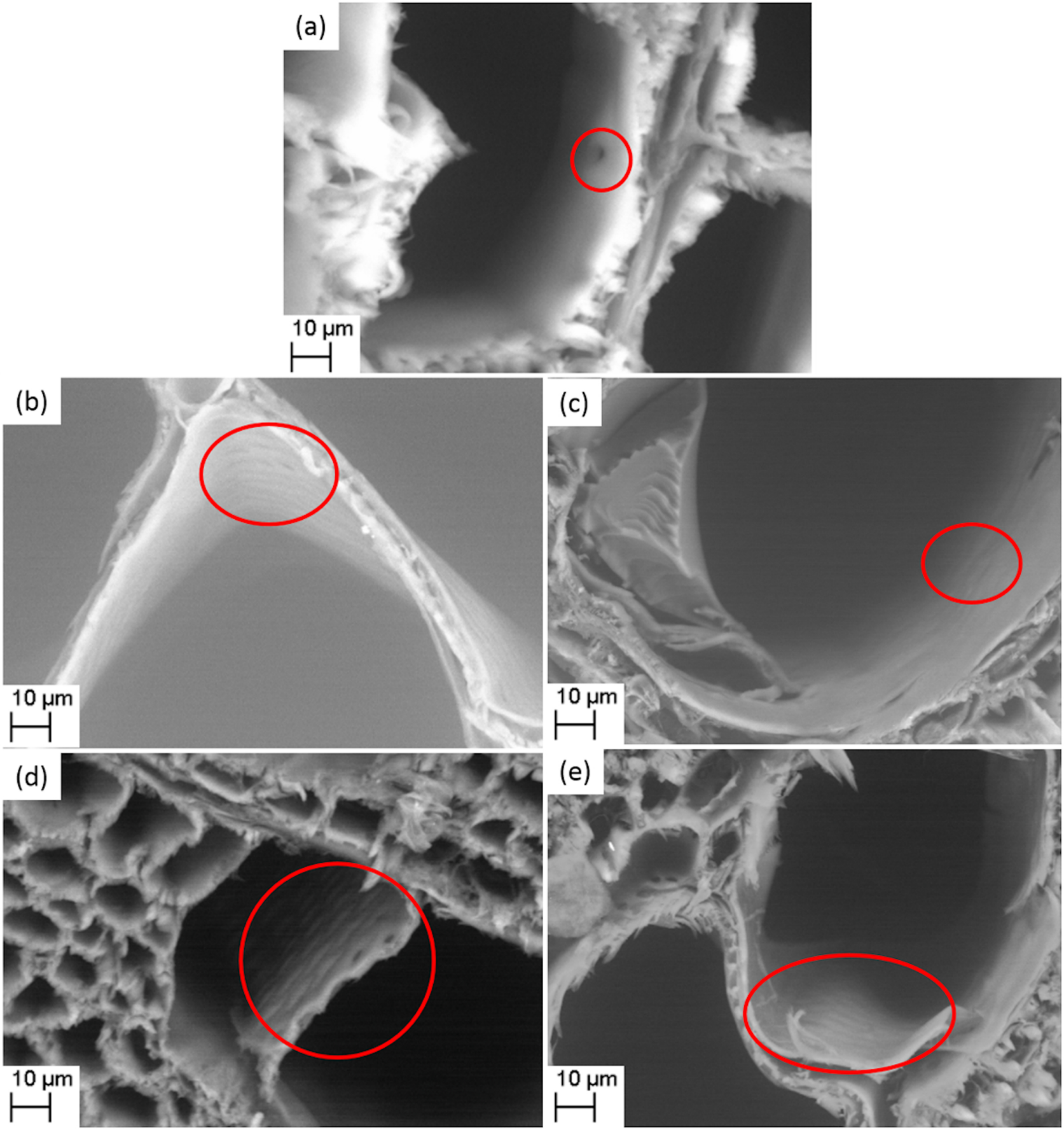

Figure 4

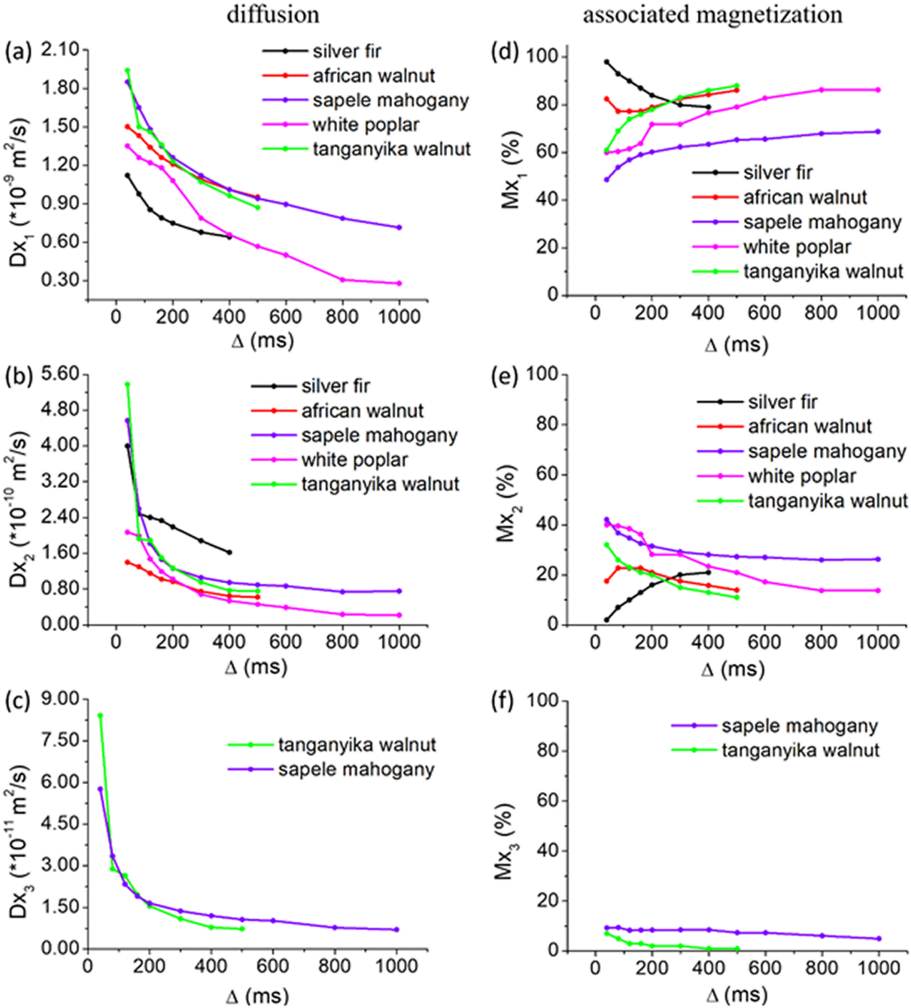
diffusion
associated magnetization
(a)
(b)
(c)
(d)
(e)
(f)
silver fir
african walnut
sapele mahogany
white poplar
tanganyika walnut
Dx1 (*10-9 m2/s)
Dx2 (*10-10 m2/s)
Dx3 (*10-11 m2/s)
Mx1 (%)
Mx2 (%)
Mx3 (%)
Δ (ms)

Figure 5

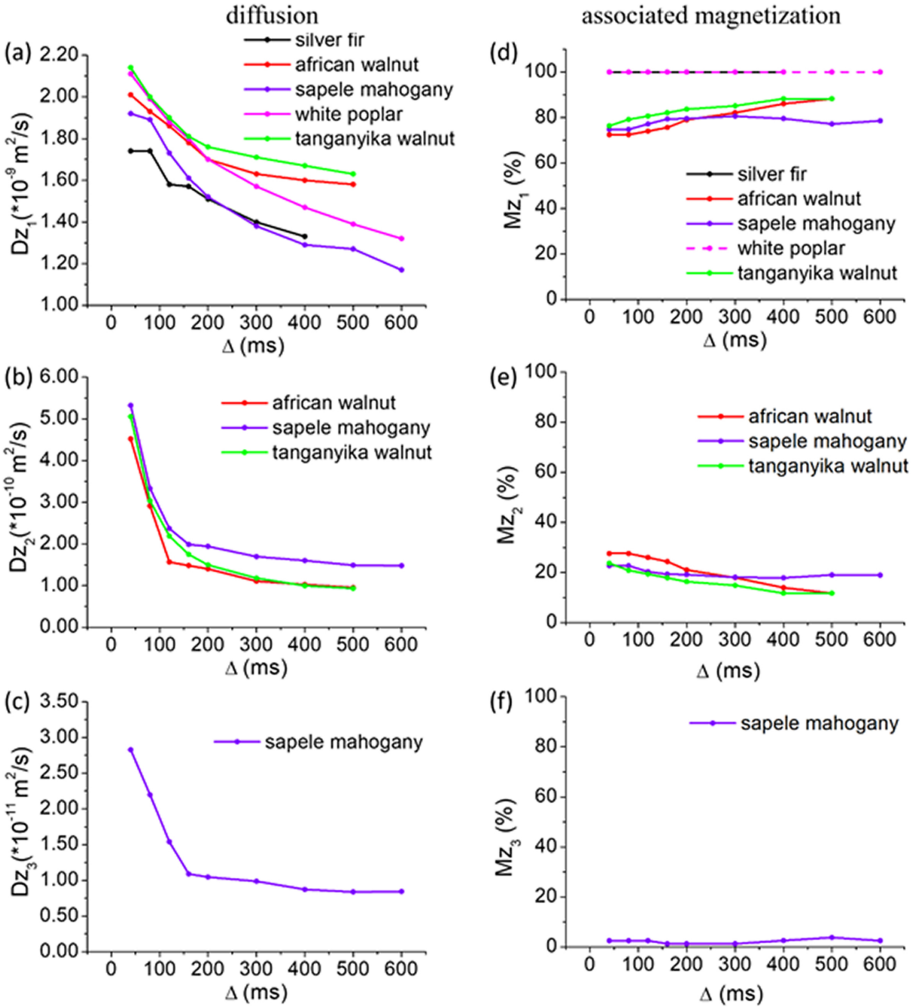
diffusion
associated magnetization
(a)
silver fir
african walnut
sapele mahogany
white poplar
tanganyika walnut
Dz1(*10-9 m2/s)
Δ (ms)
(b)
african walnut
sapele mahogany
tanganyika walnut
Dz2(*10-10 m2/s)
Δ (ms)
(c)
sapele mahogany
Dz3(*10-11 m2/s)
Δ (ms)
(d)
silver fir
african walnut
sapele mahogany
white poplar
tanganyika walnut
Mz1 (%)
Δ (ms)
(e)
african walnut
sapele mahogany
tanganyika walnut
Mz2 (%)
Δ (ms)
(f)
sapele mahogany
Mz3 (%)
Δ (ms)

Figure 6

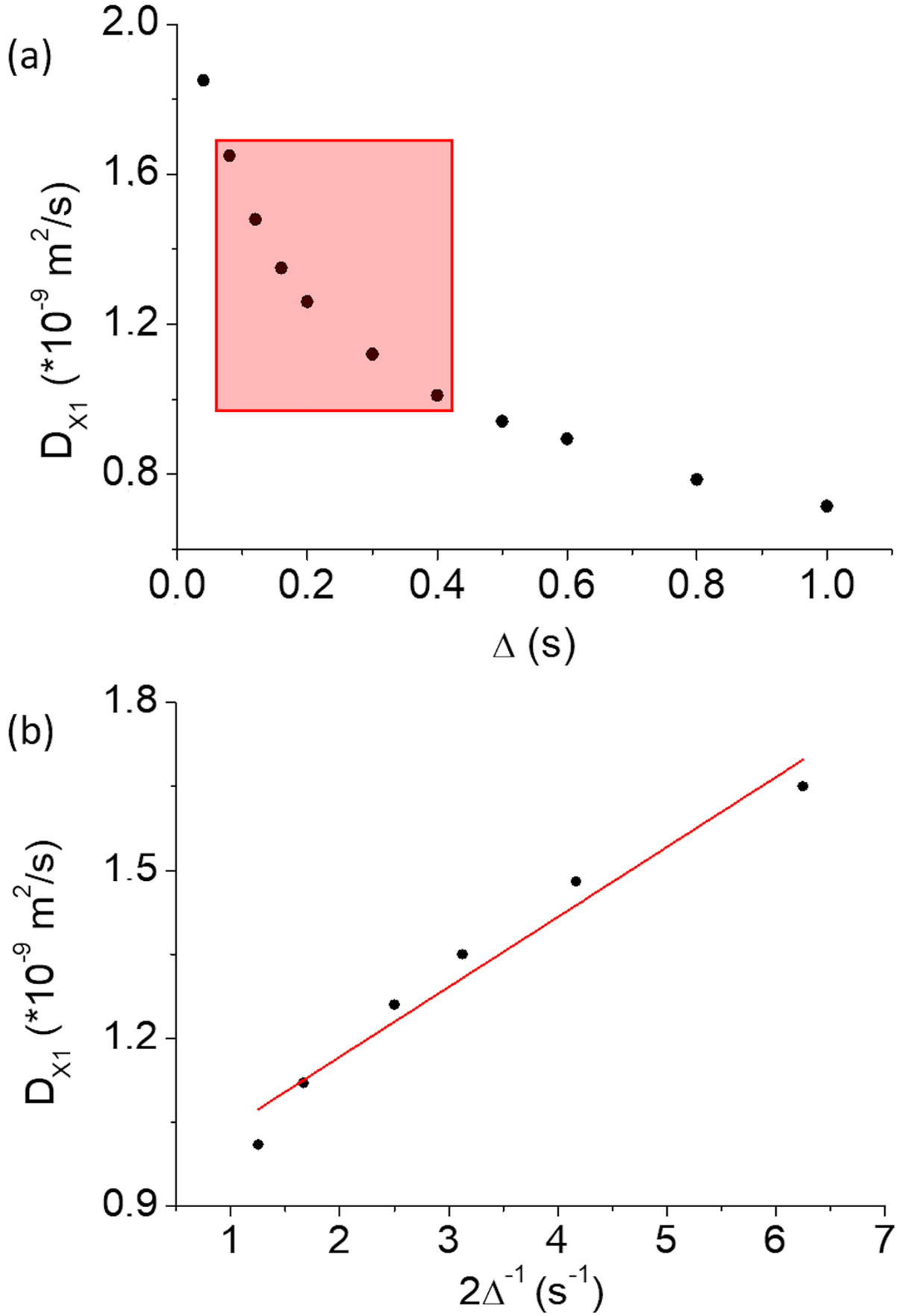
(a)
2.0
1.6
1.2
0.8
D_{X1} (*10^{-9} m^2/s)
0.0
0.2
0.4
0.6
0.8
1.0
Δ (s)
(b)
1.8
1.5
1.2
0.9
D_{X1} (*10^{-9} m^2/s)
1
2
3
4
5
6
7
$2\Delta^{-1}$ (s^{-1})

Figure 7

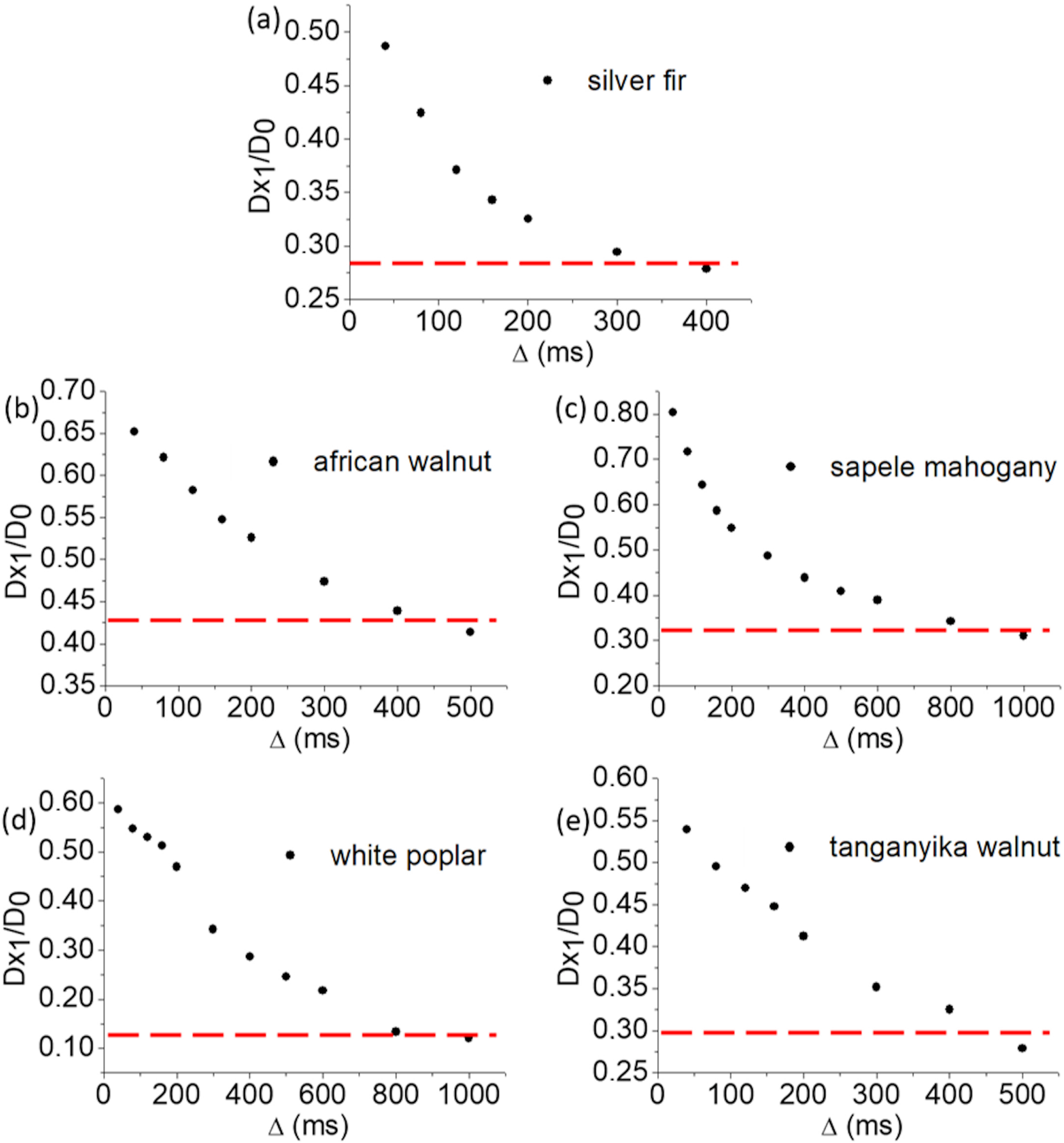
(a)
silver fir
Dx1/D0
Δ (ms)
(b)
african walnut
(c)
sapele mahogany
(d)
white poplar
(e)
tanganyika walnut

Figure 8

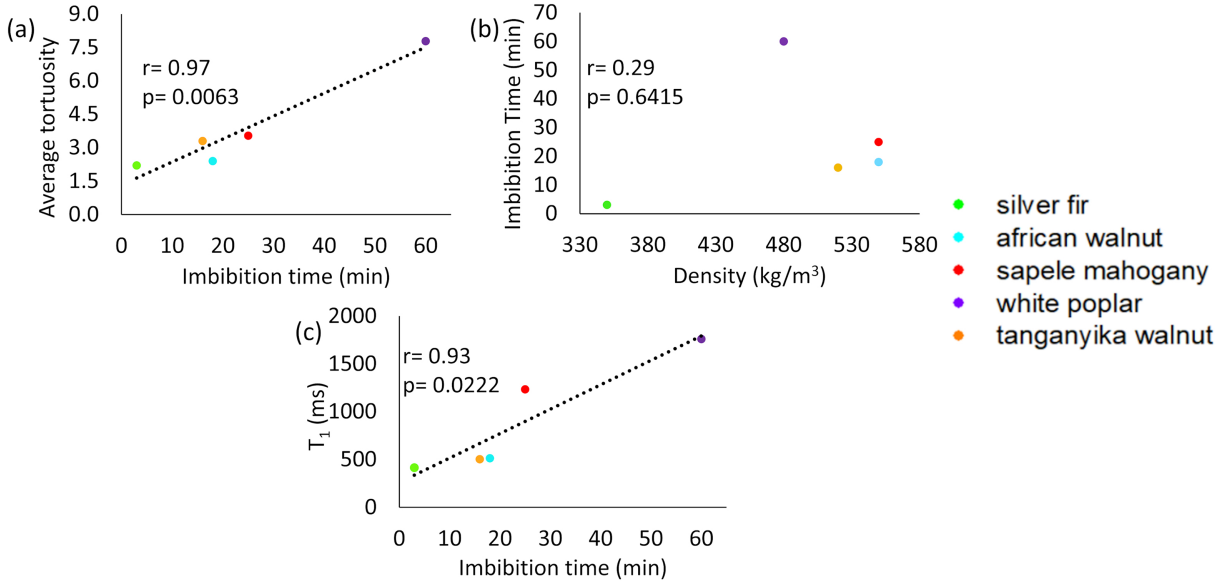
(a)
Average tortuosity
9.0
7.5
6.0
4.5
3.0
1.5
0.0
r= 0.97
p= 0.0063
0
10
20
30
40
50
60
Imbibition time (min)
(b)
Imbibition Time (min)
70
60
50
40
30
20
10
0
r= 0.29
p= 0.6415
330
380
430
480
530
580
Density (kg/m3)
silver fir
african walnut
sapele mahogany
white poplar
tanganyika walnut
(c)
T1 (ms)
2000
1500
1000
500
0
r= 0.93
p= 0.0222
0
10
20
30
40
50
60
Imbibition time (min)

Figure 9

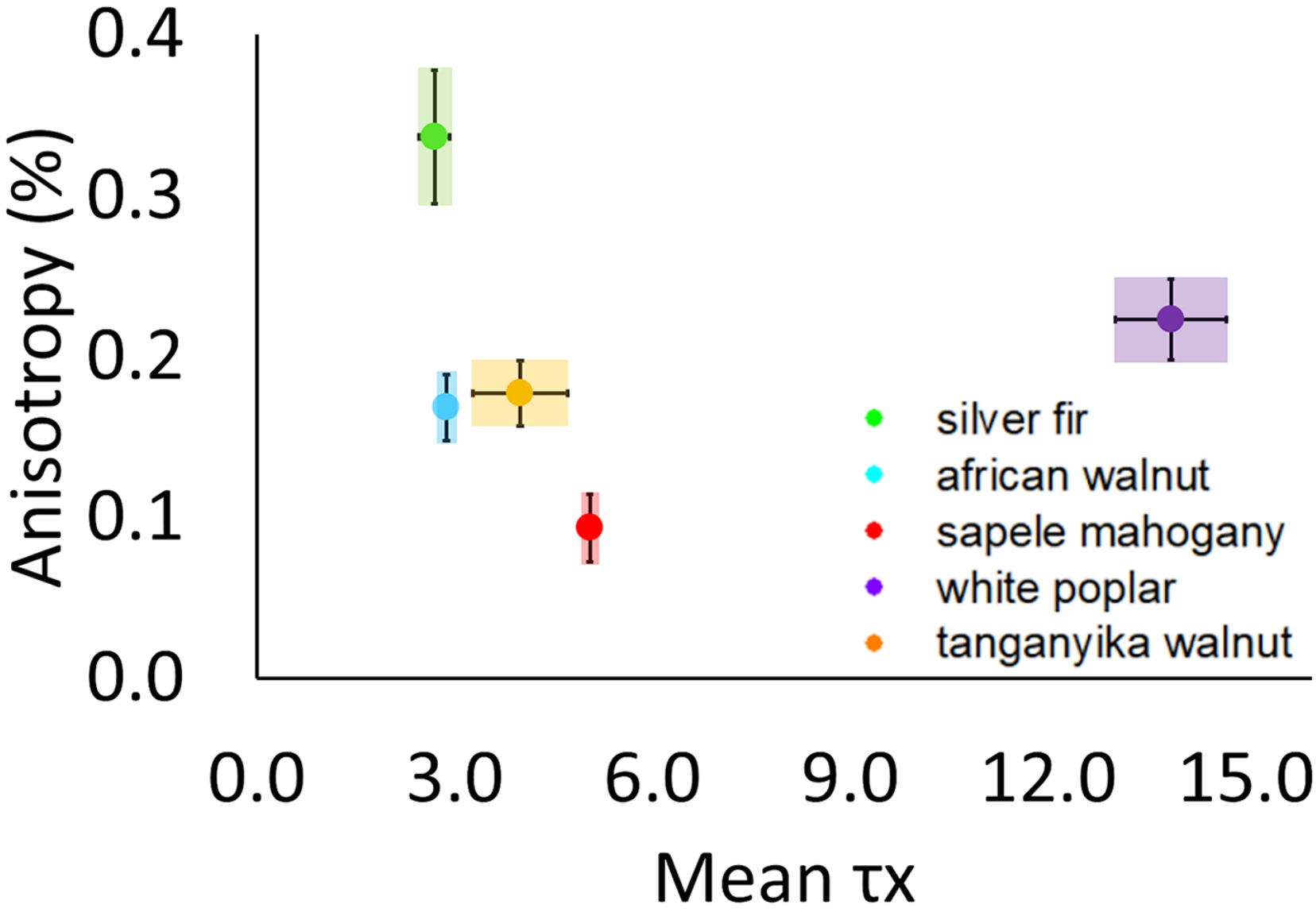
0.4
0.3
0.2
0.1
0.0
Anisotropy (%)
0.0
3.0
6.0
9.0
12.0
15.0
Mean τx
silver fir
african walnut
sapele mahogany
white poplar
tanganyika walnut

Figure 10